Molecular Cell
Article

The Three-Dimensional Architecture of a Bacterial Genome and Its Alteration by Genetic Perturbation

Mark A. Umbarger,[1,8,*] Esteban Toro,[2,8] Matthew A. Wright,[1] Gregory J. Porreca,[1] Davide Baù,[4] Sun-Hae Hong,[2,3] Michael J. Fero,[2] Lihua J. Zhu,[5] Marc A. Marti-Renom,[4,*] Harley H. McAdams,[2] Lucy Shapiro,[2] Job Dekker,[5,6,7,*] and George M. Church[1]

[1]Department of Genetics, Harvard Medical School, Boston, MA 02115, USA
[2]Department of Developmental Biology, School of Medicine
[3]Department of Physics, School of Humanities and Sciences
Stanford University, Stanford, CA 94305, USA
[4]Structural Genomics Laboratory, Bioinformatics and Genomics Department, Centro de Investigación Príncipe Felipe, 46012 Valencia, Spain
[5]Program in Gene Function and Expression
[6]Department of Biochemistry and Molecular Pharmacology
[7]Program in Systems Biology
University of Massachusetts Medical School, Worcester, MA 01605, USA
[8]These authors contributed equally to this work
*Correspondence: umbarger@post.harvard.edu (M.A.U.), mmarti@cipf.es (M.A.M.-R.), job.dekker@umassmed.edu (J.D.)
DOI 10.1016/j.molcel.2011.09.010

SUMMARY

We have determined the three-dimensional (3D) architecture of the *Caulobacter crescentus* genome by combining genome-wide chromatin interaction detection, live-cell imaging, and computational modeling. Using chromosome conformation capture carbon copy (5C), we derive ~13 kb resolution 3D models of the *Caulobacter* genome. The resulting models illustrate that the genome is ellipsoidal with periodically arranged arms. The *parS* sites, a pair of short contiguous sequence elements known to be involved in chromosome segregation, are positioned at one pole, where they anchor the chromosome to the cell and contribute to the formation of a compact chromatin conformation. Repositioning these elements resulted in rotations of the chromosome that changed the subcellular positions of most genes. Such rotations did not lead to large-scale changes in gene expression, indicating that genome folding does not strongly affect gene regulation. Collectively, our data suggest that genome folding is globally dictated by the *parS* sites and chromosome segregation.

INTRODUCTION

The three-dimensional (3D) architecture of the genome both reflects and regulates its functional state (Dekker, 2008; Thanbichler and Shapiro, 2006a). For example, chromosome segregation impacts bacterial locus subcellular positioning (Jun and Mulder, 2006; White et al., 2008), and chromatin loops that place promoters and distant enhancers within close spatial proximity play important roles in eukaryotic transcriptional regulation (Tolhuis et al., 2002; Vernimmen et al., 2007). Such examples suggest that studies of the high-resolution folding of genomes will yield insight into genome biology. However, until recently such studies, which require comprehensive assessments of the spatial positioning of many loci, have represented major technical challenges.

The recent development of several high-throughput technologies, including automated fluorescent imaging (Viollier et al., 2004) and chromosome conformation capture (3C)-based approaches (Dekker et al., 2002; Dostie et al., 2006; Duan et al., 2010; Fullwood et al., 2009; Lieberman-Aiden et al., 2009; Simonis et al., 2006; Zhao et al., 2006), has begun to enable studies of genome-wide chromosome folding. Fluorescent microscopy-based approaches allow the accurate determination of the subcellular positions of increasing numbers of defined chromosomal loci, while high-throughput 3C-based approaches enable quantification of interloci interaction frequencies that can subsequently be used to infer the average 3D distances between these loci. Studies utilizing one or both of these approaches have highlighted the potential of genome-wide studies of chromosome structure and have begun to reveal specific features of chromosome folding, including the transcription-based compartmentalization of the human nucleus (Lieberman-Aiden et al., 2009; Simonis et al., 2006) and the correlation between a locus' genomic and subcellular positioning in bacteria (Nielsen et al., 2006; Teleman et al., 1998; Wang et al., 2006b). However, the detailed structures of genomes are only beginning to be revealed, and many details, including the identities of the sequence elements that define such structures, await further elucidation.

We sought to determine the high-resolution 3D structure of an entire genome and to utilize the resulting structure to identify the sequence elements that define its architecture. Toward this goal, we studied the synchronizable bacterium, *Caulobacter crescentus* (hereafter *Caulobacter*), whose single circular chromosome is organized such that the origin and terminus of replication reside near opposite poles of the cell and other loci lie

along the long axis in an order correlating with their genomic distance from the origin (Viollier et al., 2004). To derive higher-resolution insights into the folding of this genome, we employed a multipronged approach, which utilized chromosome conformation capture carbon copy (5C) (Dostie et al., 2006), 3D modeling (Baù et al., 2011), and live-cell imaging. Using 5C, we measured 28,730 contact frequencies between loci spanning the entire *Caulobacter* genome and used these frequencies to derive 3D models of the genome in wild-type and genetically modified strains. Coupling these data with automated fluorescent microscopy, we oriented our models with respect to specific cellular landmarks. Our models demonstrate that the chromosome is ellipsoidal, with periodically arranged arms. Moreover, our 5C and microscopy data indicate that changing the position of a short (10 kb) region including the *parS* sites affects the orientation of the entire chromosome within the cell.

RESULTS

Generation of a Whole-Genome Contact Map for the *Caulobacter* Chromosome

Spatial distances between genomic loci can be inferred from the frequencies at which these loci physically interact within a population of cells. Closely positioned regions of the genome contact frequently, while spatially distant regions rarely contact. To determine the frequency of such interactions, we used 3C technology (Dekker et al., 2002), which utilizes crosslinking with formaldehyde in conjunction with spatially constrained ligation to assess the average spatial proximity of genomic loci (Figure 1A). Each 3C experiment yields a genome-wide library of ligation products whose frequencies reflect the 3D structure of the genome.

We developed a 3C protocol optimized for bacteria and employed it to generate ligation product libraries from *Caulobacter* swarmer cells, one of *Caulobacter*'s two cell types. To ascertain whether these libraries accurately reflect the spatial arrangement of the genome, we determined whether the frequencies of particular ligation products within these libraries (contact frequencies) were consistent with known features of the *Caulobacter* genome spatial organization. *Caulobacter* swarmer cells contain a single ~4 Mb circular chromosome that is divided into a left and right arm by a diametrically opposing origin and terminus of replication, which reside near opposite cell poles (Viollier et al., 2004). Thus, the origin and terminus should rarely interact. We used PCR to determine the frequency of ligation products (contact frequencies) between the origin and terminus and found that, as expected, the contact frequencies *between* loci positioned near the origin and terminus were significantly lower (<256 times) than contact frequencies between neighboring loci *within* the origin and terminus regions (Figure 1B). Thus, we conclude that 3C libraries accurately reproduce established features of *Caulobacter* genome spatial organization.

We next used 5C (Dostie et al., 2006) to comprehensively determine the composition of our swarmer 3C libraries. 5C uses highly multiplexed ligation-mediated amplification of pairs of plus- and minus-strand probes to measure the relative frequencies of tens of thousands of 3C ligation products in parallel. In our modified 5C approach, bar-coded oligonucleotide probes were used to specifically detect and amplify ligation junctions between restriction fragments, and the frequency of such junctions was quantified by polony-sequencing of the ligated probe pairs (Shendure et al., 2005) (Figures 1A and S1A).

To interrogate the *Caulobacter* genome at high density, we designed 339 5C probes with 169 complementary to the plus- and 170 complementary to the minus-strand of restriction fragments (Figure 1C). These probes cover the *Caulobacter* genome in an alternating fashion, with adjacent fragments queried by opposite strand probes, enabling the measurement of 28,730 contact frequencies and the sampling of the *Caulobacter* genome at an average resolution of ~13 kb (σ = 13 kb).

We generated genome-wide 5C libraries for synchronous *Caulobacter* swarmer cells and found that the resulting contact frequencies were highly correlated across replicates ($r > 0.94$, Table S1), indicating a high degree of reproducibility of individual contact frequencies. We collectively represent these frequencies as two-dimensional contact maps in which the plus- and minus-strand-probed restriction fragments are ordered along orthogonal axes. The contact frequency between any given pair of fragments is thus located at the intersection of the corresponding row and column (Figure 1D).

The Swarmer Cell Chromosome Is Ellipsoidal with Specific Regions at the Poles

The swarmer cell 5C contact map contains two prominent diagonals that intersect near the center (the terminus region, 2 Mb) and corners (the origin region, 0/4 Mb) of the map (Figure 1D). To understand the structural implications of these diagonals, it is helpful to consider what such a map would look like for an unconstrained circular chromosome. In such a structure, interactions would exclusively occur between loci proximal in the genome, yielding a contact map with a single diagonal stretching from the upper left to lower right corners (Figures S1B and S1C). In addition to this diagonal, the swarmer cell contact map contains a second diagonal from the lower left to the upper right corner, indicating the presence of prominent interactions between fragments separated by large genomic distances. Correspondingly, the contact frequency profiles of most fragments contain a peak of short-range interactions centered about the genome coordinates of these fragments as well as a second peak of long-range interactions. Interestingly, these long-range interactions are centered about loci on the opposite arm that are roughly equidistant from the origin (Figure 1E). Collectively, these short- and long-range peaks indicate that the swarmer cell chromosome structure is ellipsoidal, with loci roughly symmetric about the origin folded close in space and a long axis connecting regions near the origin and terminus (Figure 1E).

The swarmer cell 5C contact map allows us to identify the maximally polar regions of the ellipsoidal swarmer cell chromosome. As these regions are approached along either arm of the chromosome, the genomic distance to the contacting region on the opposite arm becomes smaller until the proximal short-range and the long-range (interarm) peaks in contact frequency profiles merge. Thus, the maximally polar regions of the genome correspond to the positions in the contact map at which the two diagonals intersect (Figure S1D). We find that one polar locus corresponds to a region near the origin and the second to a

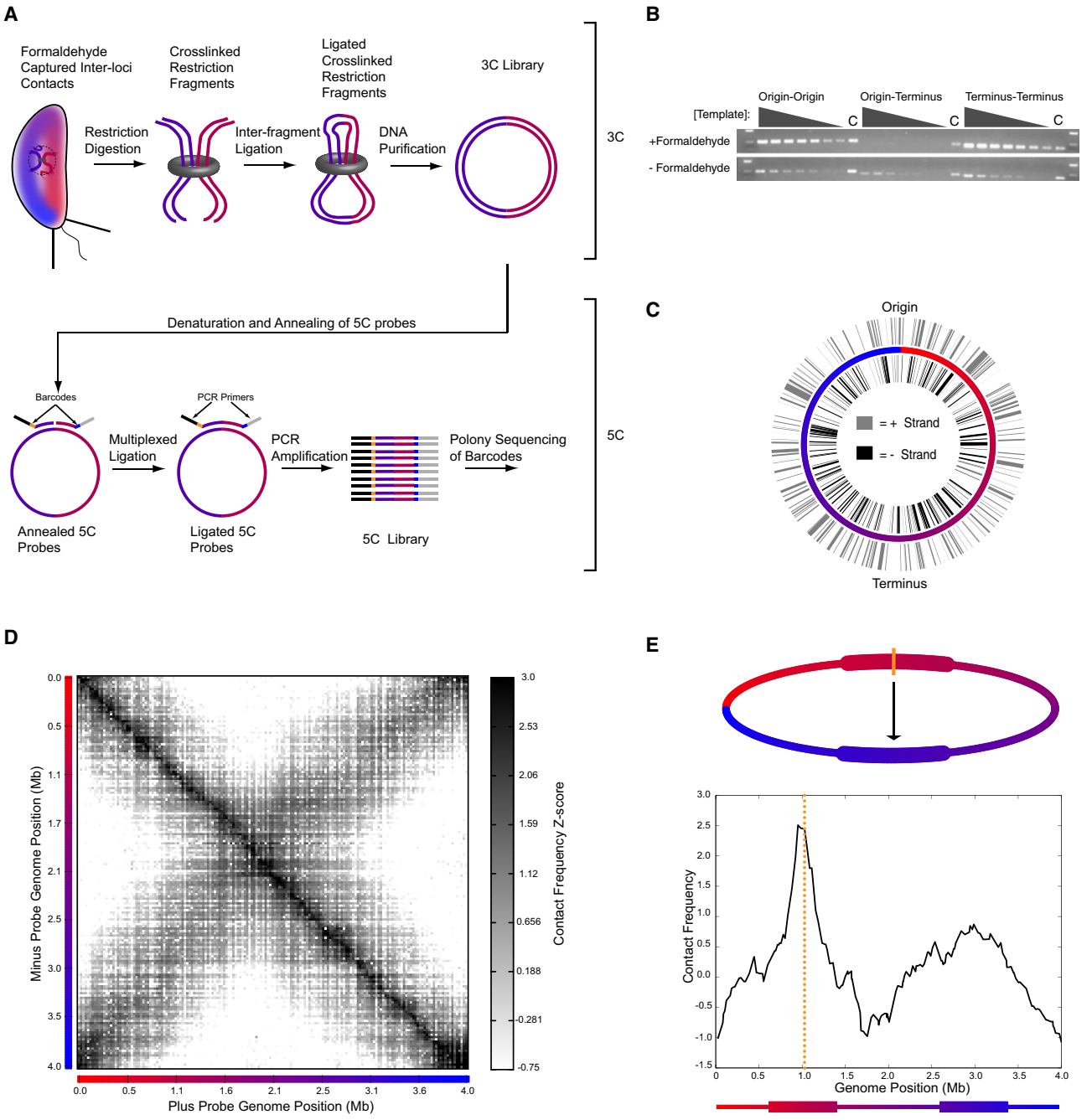

Figure 1. Genome-wide 5C Reveals that the Swarmer Chromosome Is Ellipsoidal

(A) Our 3C and 5C approaches. Top: Formaldehyde is added to synchronized swarmer cells, crosslinking physically touching chromosomal loci (e.g., the red and purple regions denoted within the dashed circle). Chromatin is subsequently digested with a restriction enzyme and is diluted to separate noncrosslinked fragments. Ligation is then performed, yielding a 3C library of ligation products in which interfragment crosslinks are now represented as ligation products between fragments. Bottom: Next, bar-coded oligonucleotide probes with sequences complementary to the ends of restriction fragments (plus or minus strand) are annealed to the 3C library. Multiplexed ligation is subsequently performed, creating carbon copy ligation products between annealed plus- and minus-strand probes that reflect the original crosslinks between restriction fragments. By design, ligation can only occur between plus- and minus-strand probes. Carbon copy junctions are subsequently amplified via PCR using the universal flanking tails, yielding a 5C library, and the frequencies of products within this library are assessed via barcode sequencing.

(B) 3C recapitulates established features of *Caulobacter* swarmer cell genome structure. Template dilution (2-fold) series PCR reactions querying ligation products among origin- and terminus-proximal restriction fragments in swarmer cell 3C libraries generated with (top) or without (bottom) fixation were performed, and the resulting products were run on an agarose ethidium bromide-stained gel. "C" denotes a control template in which junctions were present in equal concentrations (see Supplemental Experimental Procedures).

region near the terminus. Thus, our data are consistent with the origin and terminus residing near opposite cell poles (Viollier et al., 2004). Importantly, the resolution of our 5C data enables a more precise definition of the genomic regions located at the extreme poles. We find that the origin-proximal maximally polar region is located 25 ± 17 kb to the left of the origin and contains the *parS* sequence elements (Livny et al., 2007; Mohl and Gober, 1997) (Figures S1E and S1F) and that the terminus-proximal maximally polar region lies 42 ± 17 kb to the left of the *dif* site (Figures S1E and S1F) (Jensen, 2006). Of note, the *parS* sites are known to act as centromere-like elements in *Caulobacter* (Toro et al., 2008), and the *dif* sites play a role in the resolution of chromosome dimers formed during replication and segregation (Jensen, 2006). Thus, our contact frequency data suggest that the chromosome is folded about sequence elements critical to chromosome segregation.

Generation of 13 kbp-Resolution 3D Models of the *Caulobacter* Chromosome

Next, we used the swarmer 5C data to generate models of the 3D conformation of the *Caulobacter* swarmer cell genome. Our 5C data represent a comprehensive set of contact frequencies between loci spanning the entire genome. It has been demonstrated that contact frequencies are reliable proxies for the average spatial distances between loci (Lieberman-Aiden et al., 2009; Miele et al., 2009), and we observed a similar relationship in our data (Figures S2A and S2B). Therefore, we can convert 5C contact frequencies into average spatial distances, which can then be used to derive 3D models.

To generate models we utilized the Integrative Modeling Platform (IMP, http://www.integrativemodeling.org) (Alber et al., 2007; Baù et al., 2011) to search for the 3D conformations of the *Caulobacter* genome that satisfy the distances inferred from our 5C contact maps (Figure 2A). This approach yields population-average conformations, which represent the dominant folding patterns across the cell population, but does not reveal the variations in detailed conformations that undoubtedly exist. Specifically, we utilized fluorescent microscopy-derived distances between hundreds of chromosomal loci located on the same arm (Figure S2B) in conjunction with 5C data to derive a calibration curve for relating contact frequencies to spatial distances (see Supplemental Experimental Procedures). We then transformed all 5C contact frequencies into average 3D spatial distances (Figure 2A, i, and Supplemental Experimental Procedures). Next, treating each restriction fragment as a point in space, we connected fragments with springs with equilibrium distances equal to the 5C-derived distances (Figure 2A, ii). The 3D coordinates of all fragments were then stochastically initialized (Figure 2A, iii), and in an iterative process that utilizes simulated annealing, the spatial locations of fragments were randomly modified until a structure that satisfied as many of the 5C-derived distances as possible was attained (Figure 2A, iv, a). We repeated this optimization 56,000 times to generate an ensemble of structures that was maximally consistent with our 5C data. Finally, we structurally superimposed and clustered the 10,000 models with the fewest violations of the distance constraints into groups of highly similar structures (Figure 2A, iv, b).

3D Modeling Yields a Single Class of Models with Periodically Arranged Arms

We find that the models of the *Caulobacter* swarmer cell chromosome group into only four structurally similar clusters (Table S2), suggesting that while the chromosome may be flexible and folded somewhat differently in each cell, there are a small number of dominant conformations. To represent the swarmer cell model clusters, we present 3D density maps in which the volume occupied by each fragment indicates the variation in this fragment's positioning across the models in the cluster (Figure 2B). Such volume elements may represent dynamic variability in a fragment's spatial positioning (Elmore et al., 2005; Fiebig et al., 2006; Reyes-Lamothe et al., 2008) and likely encompass local structures such as topological domains, which are below the resolution of our data (Postow et al., 2004).

In 3D coordinate space, we find that the differences between models are largely the result of mirroring of portions of the structures. The presence of mirrors is expected, as perfect mirror images are indistinguishable by 5C and are equivalent in distance space. Indeed, clusters 1 and 2 as well as clusters 3 and 4 are pairs of nearly perfect mirror images (Figure S2D). Furthermore, clusters 1 and 2 are partial mirrors of clusters 3 and 4 (Figure S2E). Thus, the four model clusters represent small variations on a single conformation.

The models within all clusters display structural features apparent from the raw contact maps: their overall geometry is ellipsoidal, with loci roughly equidistant from the origin folded close in space. The origin-proximal maximally polar fragment is located ~7 kb to the left of the *parS* elements (Figure 2C and Table S2), which is within the resolution of 5C data (~13 kb). Based on fragment intracluster variability, we determined that the effective resolution of the models is between 175 and 225 nm (Figure S2C). We expect that the actual resolution of individual models may be much higher, as models may be locally very similar along their length but diverge significantly at a few positions.

(C) 5C whole-genome coverage map. The central circle represents the *Caulobacter* genomic map, with coloring indicating genome position (from red to blue). The interior and exterior circles represent the genomic locations of restriction fragments queried by plus- (gray exterior) and minus- (black interior) strand 5C probes.

(D) Average swarmer cell 5C contact map. The frequency of a junction between a given pair of fragments in the library (contact frequency) is found at the intersection of the row and column corresponding to the fragments. Minus- and plus-strand-probed restriction fragments are ordered according to genome position along the vertical and horizontal axes, respectively. The origin is located at 0 Mb, and the terminus is located at ~2 Mb. Bars underneath and to the left of the two axes indicate genome position. Color within the heat map is indicative of the contact frequency Z score (see Supplemental Experimental Procedures).

(E) Bottom: The contact frequency profile for a representative fragment located at ~1 Mb. This profile indicates the contact frequencies for a given fragment with all other fragments of opposite type and corresponds to a row of the contact map. The orange dotted line indicates the genome coordinate of this fragment. Top: Schematic of the ellipsoidal geometry suggested by the contact frequency profile shown below. Figure S1 provides the corresponding profile and contact map if the chromosome were an unconstrained circle.

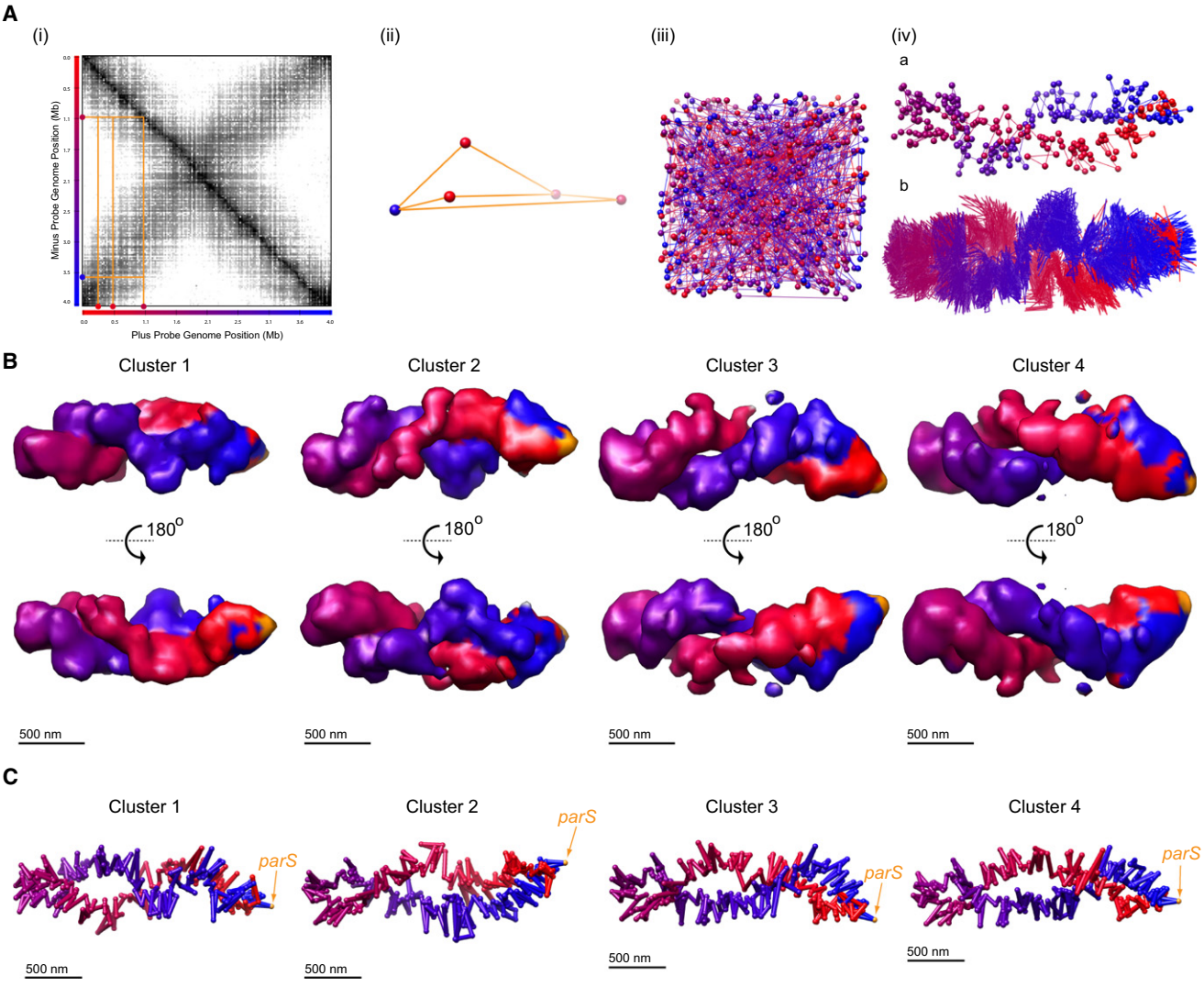

Figure 2. Modeling Reveals the 3D Architecture of the Swarmer Genome

(A) Outline of our modeling methodology. Restriction fragments were modeled as points connected by springs. The distance derived from the contact frequency between pairs of fragments was used (i) to define the equilibrium length of the spring (see Supplemental Experimental Procedures) that connected these fragments (ii). The 3D coordinates of all points were randomly initialized (iii), and optimization was performed to derive a structure that minimally violates these equilibrium lengths (iv, a). This initialization and optimization procedure was repeated thousands of times to generate an ensemble of structures. These structures were superimposed and grouped based upon their coordinates, yielding clusters of models in which the 3D coordinates of restriction fragments are structurally very similar (iv, b).

(B) 3D density map representations of the four clusters from a wild-type swarmer modeling run. Each queried fragment is represented by a 3D Gaussian that has a correlation coefficient >0.8 with the space this fragment occupies across all models within the cluster. The positioning of the maximally polar fragment (located ~7 kb from the *parS*) elements is indicated in orange.

(C) The centroid model of swarmer clusters 1–4. For more information regarding these clusters, see Figure S2 and Table S2.

A prominent feature emerges from all four clusters: the arms are wound sinusoidally through space with roughly 1.5 period repeats per arm. The partial mirroring between clusters 1 and 2 and clusters 3 and 4 has the effect of causing the arms to be either intertwined (clusters 3 and 4) or separated (clusters 1 and 2). We favor the intertwined conformation, as the corresponding model clusters have lower variability (Figure S2C) and lower IMP objective function scores (Table S2). However, it is possible that both conformations exist within a population of swarmer cells.

The *parS* Region Dictates the Orientation of the Entire *Caulobacter* Chromosome

Our models suggest that the *parS* sites play a direct role in organizing the swarmer cell chromosome. Such a finding is consistent with recent analyses that have suggested that these sequence elements are specifically anchored to the *Caulobacter* old cell pole through interactions with the ParB and PopZ proteins (Bowman et al., 2008; Ebersbach et al., 2008; Toro et al., 2008). Thus, we hypothesized that the orientation of the

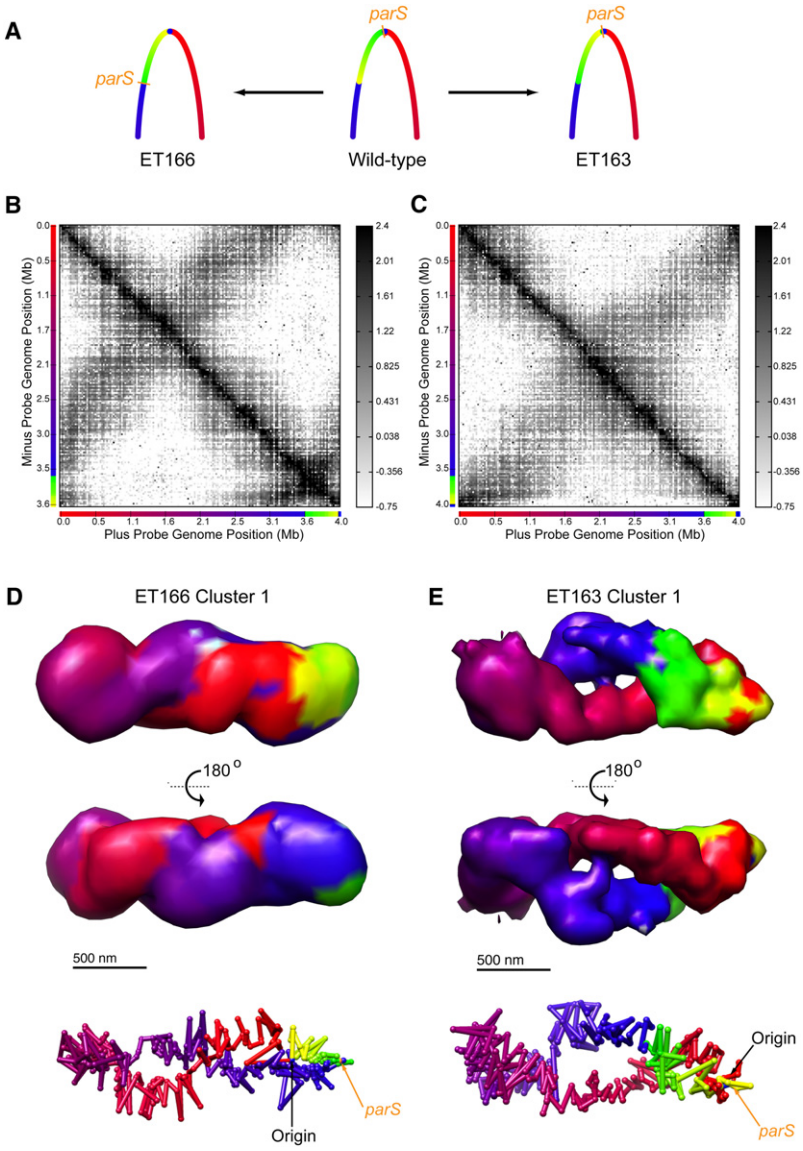

Figure 3. 5C Analyses of Strains Carrying Genomic Inversions Reveal that the *parS* Elements Are Critical to Defining Chromosome Orientation

(A) Genomic maps for strain CB15N (wild-type) and inversion strains ET166 and ET163. The inverted region is indicated in yellow and green.

(B and C) Contact maps for strain ET166 and ET163 swarmer cells.

(D and E) 3D density map (top) and cluster centroid (bottom) representations for the two largest ET166 and ET163 model clusters (see Figures S3A and S3C for representations of the two additional clusters for each strain). The *parS* elements are located near the junction of the blue and green portions of the ET166 models and near the junction of the yellow and red regions of the ET163 models.

entire *Caulobacter* chromosome is defined by *parS*-based anchoring. To test this hypothesis, we studied an inversion strain (ET166) in which the *parS* sites were moved ~400 kb away from the origin (Figure 3A). We performed 5C on this strain and discovered that the resulting contact map displays a marked displacement of the diagonal representing contacts between the two arms toward the upper left corner (Figure 3B), indicating a change in the pattern of interactions between opposite arm loci. 3D models generated using these data show a striking genome-wide clockwise rotation of loci within the ellipsoidal structure, thereby positioning the *parS* sites at a structural pole (Figures 3C and S3A and Table S3). Thus, changing the position of the *parS* sites in the genome resulted in a large-scale reorganization of its 3D architecture. This dramatic reorientation of the chromosome was not observed in a control strain, ET163, which carried a similar but slightly smaller (by 10 kb) inversion that did not change the positions of the *parS* sites (Figures 3A, 3D, 3E, and S3C). Therefore, we conclude that the rotation observed in ET166 was a direct result of moving the 10 kb region containing *parS* sites (*parS* region, hereafter) to a new genomic location.

Live-Cell Imaging Confirms that the *parS* Region Establishes Global Chromosome Organization within the Cell

5C-derived contact frequencies reflect the relative positions of loci but do not indicate the subcellular positions at which contacts occur. Thus, we next turned to in vivo microscopy to place the observed structures within the context of the cell. Starting with the inversion strains described above, we generated a set of derivative strains that had *lacO* arrays inserted at different chromosomal locations, thereby allowing us to utilize LacI-CFP fusion proteins to visualize the subcellular positions of these loci in living cells (Figure 4A).

We first measured the subcellular positions of over 60 different loci in at least 500 wild-type cells. The resulting images illustrate that loci on the same arm are arranged in a roughly linear fashion along the long axis of the cell (Figure 4B) and hence are consistent with both our models as well as previous microscopy data (Viollier et al., 2004). We next analyzed the inversion strains and confirmed that in strain ET166, in which the *parS* sites were located ~400 kb away from the origin, the entire chromosome did in fact rotate in a clockwise fashion within the cell (Figure 4B). Such a rotation was not observed in the control strain, ET163, which displayed only a subtle rotation of loci in the opposite direction (Figure 4C). Importantly, the terminus region was among the portions of the genome whose subcellular position was changed in ET166 relative to wild-type, indicating that, as our 3D models predicted, the terminus is not anchored to a pole of the cell.

To confirm the importance of the *parS* region in shaping the organization of the swarmer cell genome, we created an additional inversion strain, ET322, in which this region was moved to the right of the origin (as opposed to ET166, where it was

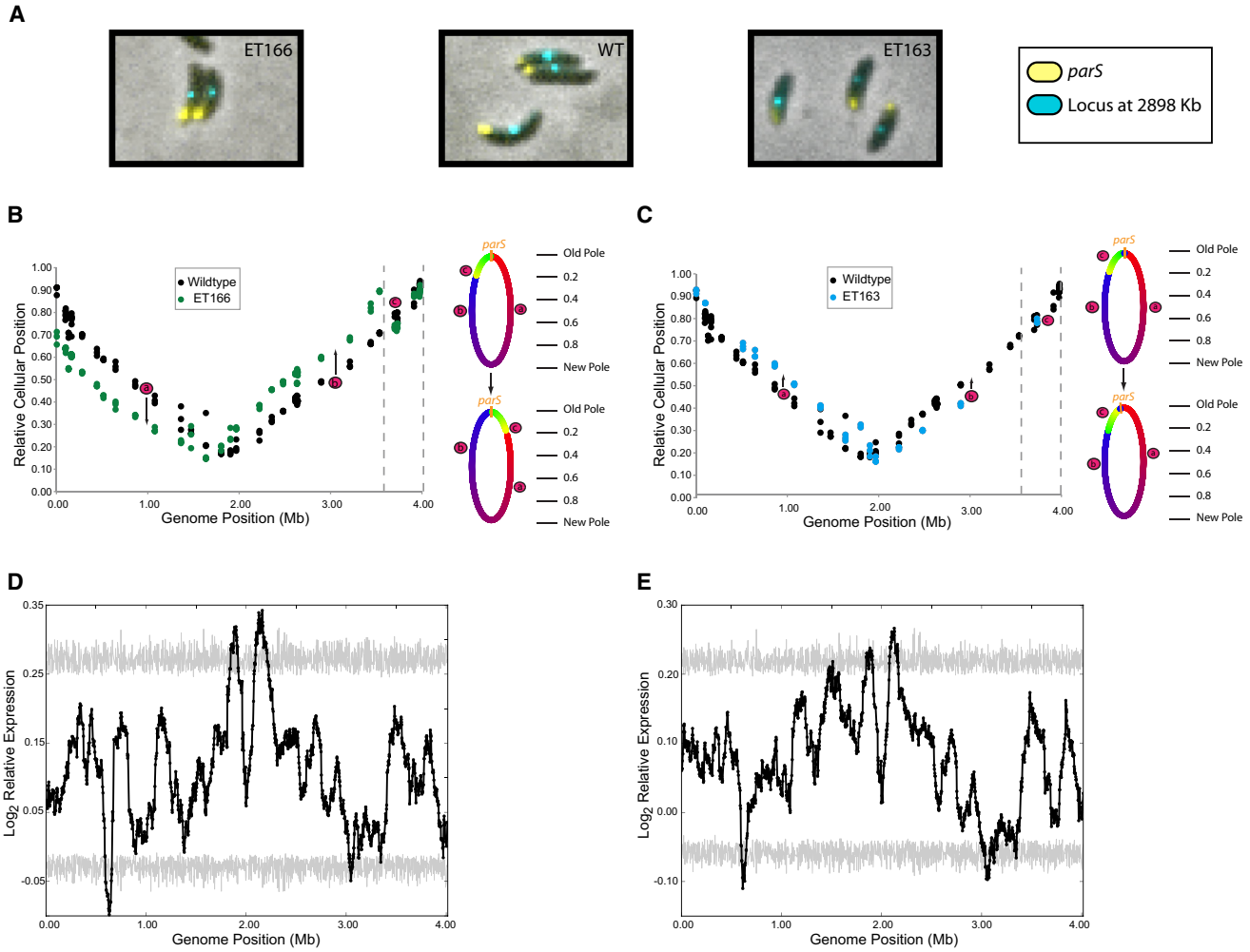

Figure 4. Moving the *parS* Sites to New Genomic Positions Leads to a Rotation of the Genome without Strongly Affecting Gene Expression

(A) Representative images showing the position of *parS* (yellow) and a *lacO* array (blue) inserted 2898 kb from the origin (cyan) in wild-type and the inversion strains ET166 and ET163.

(B and C) Subcellular localization of DNA loci bearing *lacO* insertions visualized with LacI-CFP in swarmer cells with a wild-type (black) or inverted (ET166-green or ET163-red) chromosome. Each point represents an independent measurement of the average cellular position of LacI-CFP in at least 100 cells. Relative cellular position was measured with respect to the old (stalked) cell pole. The dotted vertical lines denote the inversion break points in strains ET166 and ET163. Cartoons to the right illustrate the gross organization and orientation of the chromosomes before and after inversion. Red points provide guides to match the cartoons to the data. See Figure S4 for data for an inversion strain in which the *parS* sites are located to the right of the origin.

(D and E) Plots of smoothed relative gene expression (75 kb half-window) versus genome position for strains ET166 and ET163. The gray lines denote the 0.001 significance thresholds (see Supplemental Experimental Procedures).

moved to the left of the origin) (Figure S4). We expected that such a positioning of the *parS* region would result in a wholesale rotation of the chromosome similar to that seen in ET166, but in the opposite direction. Indeed, we find that in this strain, the *parS* region remains at the pole, while the rest of the chromosome, including the terminus, rotated as expected (Figure S4).

Thus, both our 3D models and live-cell imaging demonstrate that the only locus whose position is fixed in the cell is the 10 kb region containing the *parS* sites. The gross orientation of the entire chromosome is determined, to a large extent, by the relative position of this region. At our current resolution, we are unable to determine whether or not additional (i.e., non-*parS*) anchor points exist within the 10 kb region we have manipulated. In fact, since ParB, the DNA-binding protein that binds to the *parS* sites, itself interacts with a number of other polarly localized proteins, including MipZ (Thanbichler and Shapiro, 2006b) and PopZ (Bowman et al., 2008; Ebersbach et al., 2008), it seems likely that the *parS* anchoring region represents a large nucleoprotein complex that encompasses tens of kilobases of sequence.

Genome Orientation Does Not Globally Affect Gene Expression

We sought to determine if the positioning of loci relative to each other and cellular landmarks globally affects gene expression. If such positioning controls expression, the gene expression

profiles of strains ET163 and ET166 should be dissimilar, as the chromosomes in these strains adopt markedly different conformations. To test this hypothesis, we isolated RNA from synchronous ET163, ET166, and wild-type swarmer cells and competitively hybridized inversion strain and wild-type RNA to Agilent microarrays.

We found that the expression profiles of ET163 and ET166 were highly correlated (R = 0.82). The transcriptional changes in these strains relative to wild-type were minor, as the expression levels of the majority of affected genes changed less than 2-fold (Table S5). Of the differentially expressed genes, over half were common between the two strains (206 of 377/386, $p < 10^{-7}$, Figure S4C), and this set was not enriched for genes whose subcellular positions changed (Table S6), indicating that most of the observed expression differences in ET163 and ET166 (relative to wild-type) were the result of the inversion common to these strains rather than changes in gene positioning. Supporting this conclusion, we found that plots of relative expression versus genome position generated using a sliding average approach are similar for ET163 and ET166 (Figures 4D and 4E). While these plots indicate that relative expression levels in both strains fluctuate with genome position, randomizations illustrate that the observed peaks and troughs are generally not statistically significant (Figures 4D and 4E). The small number of regions whose expression levels do exceed the confidence threshold, however, are common between the two strains (Figures 4D and 4E), again illustrating that the observed expression changes are the result of the inversion. Thus, our expression data indicate that despite significant differences in the 3D conformations of their genomes, ET163 and ET166 have similar expression profiles. We conclude that locus repositioning does not globally affect gene expression.

Alignments of the Chromosomal Arms Reveal the Presence of Additional Constraints on Genome Structure

To assess whether there exist additional constraints on chromosome folding outside of the *parS* region, we wished to determine whether the arms of the chromosome run in register from pole to pole. If the arms were to run in parallel along the long axis without additional constraints, we would expect that opposite-arm loci positioned at similar genomic distances from the *parS* sites would be located at similar positions along the long axis of the structure. Thus, for each fragment in each model, we identified the closest opposite-arm fragment with respect to positioning along the long axis of the models and then compared the genomic distances of these loci to the *parS* sites (the maximally polar loci). For the majority of the wild-type genome, we find that the closest opposite-arm fragments are indeed roughly equidistant from the *parS* sites, with a small deviation from symmetry near the opposite pole (Figure 5A). Thus, our models indicate that the arms of the wild-type swarmer cell chromosome are well aligned.

We performed a similar analysis for strain ET166, the inversion strain in which the *parS* sites were moved ~400 kb to the left of the origin. Interestingly, we find that despite the fact that much of the genome rotates in register, placing the *parS* region at a structural pole, there are a large number of loci located outside of the inverted region, which despite residing at different genomic distances from the *parS* sites are aligned along the long axis of the cell (Figure 5B). A similar and more extreme lack of symmetry was also observed in the models for strain ET163, the inversion strain in which the *parS* sites remained near the origin (Figure S5A). Such findings suggest that there are additional factors (see Discussion), possibly located within the inverted regions, which control the positioning of the chromosomal arms.

The *parS* Sites and Polar Localization Drive the Formation of Compact Chromatin Domains

We next used our models to assess if the swarmer cell genome is uniformly compacted along its length, or if instead there are regions of unusual compaction, as has been observed in other systems (Gilbert et al., 2004; Mercier et al., 2008). The average distance among sets of neighboring loci in compact regions should be smaller than the corresponding distances in less tightly packed regions. Therefore, we can utilize the mean distance between neighboring loci in a model as a measure of compaction. To ensure that such a measure accurately reflects compaction, we first corrected the observed interfragment distances for differences in genomic site separation. Specifically, for each model we utilized the mean relationship between intra-arm site separation and spatial distance to define expected interloci distances. We then calculated the log ratios of these expected distances to the observed distances and determined the average log ratios for sets of neighboring fragments, defining compaction scores (Gheldof et al., 2006). This process was repeated for each model in our clusters, and the cluster-wide average compaction scores were plotted against genome position. It is worth highlighting that these scores reflect the 3D distances between fragments rather than protein density on DNA, a parameter frequently measured by nuclease sensitivity and density gradient centrifugation assays. While protein density and interloci distances are likely correlated, it is conceivable that regions of low protein density could be located close in space.

We found that in wild-type cells, fragments located near both poles showed above-average levels of compaction (Figures 6A and 6B). When these regions were moved away from the poles as a result of the inversion in strain ET166, they became less compact (Figures 6A and 6C). Correspondingly, the compaction level of loci moved toward the poles increased. A similar, though more moderate, change in compaction was observed for genomic regions moved closer to the *parS* pole in ET163 (Figure S5B). Thus, we conclude that polar localization, perhaps due to the more constrained geometry of the cell poles, can lead to the formation of a compact chromatin conformation.

Interestingly, we observed that the regions to the left of the *parS* sites were arranged in a particularly compact fashion (Figures 6A and S5B). Two lines of evidence indicate that polar localization alone does not entirely explain such compaction. First, we observe that in ET166, the compaction level of the region moved closer to the *parS* sites increases significantly more than the region moved closer to the opposite pole (Figure 6A). Second, while in both wild-type and ET166 cells there are regions near the poles opposite the *parS* sites that are arranged somewhat compactly, these regions are asymmetrically positioned with respect to these poles (Figure 6B). Such

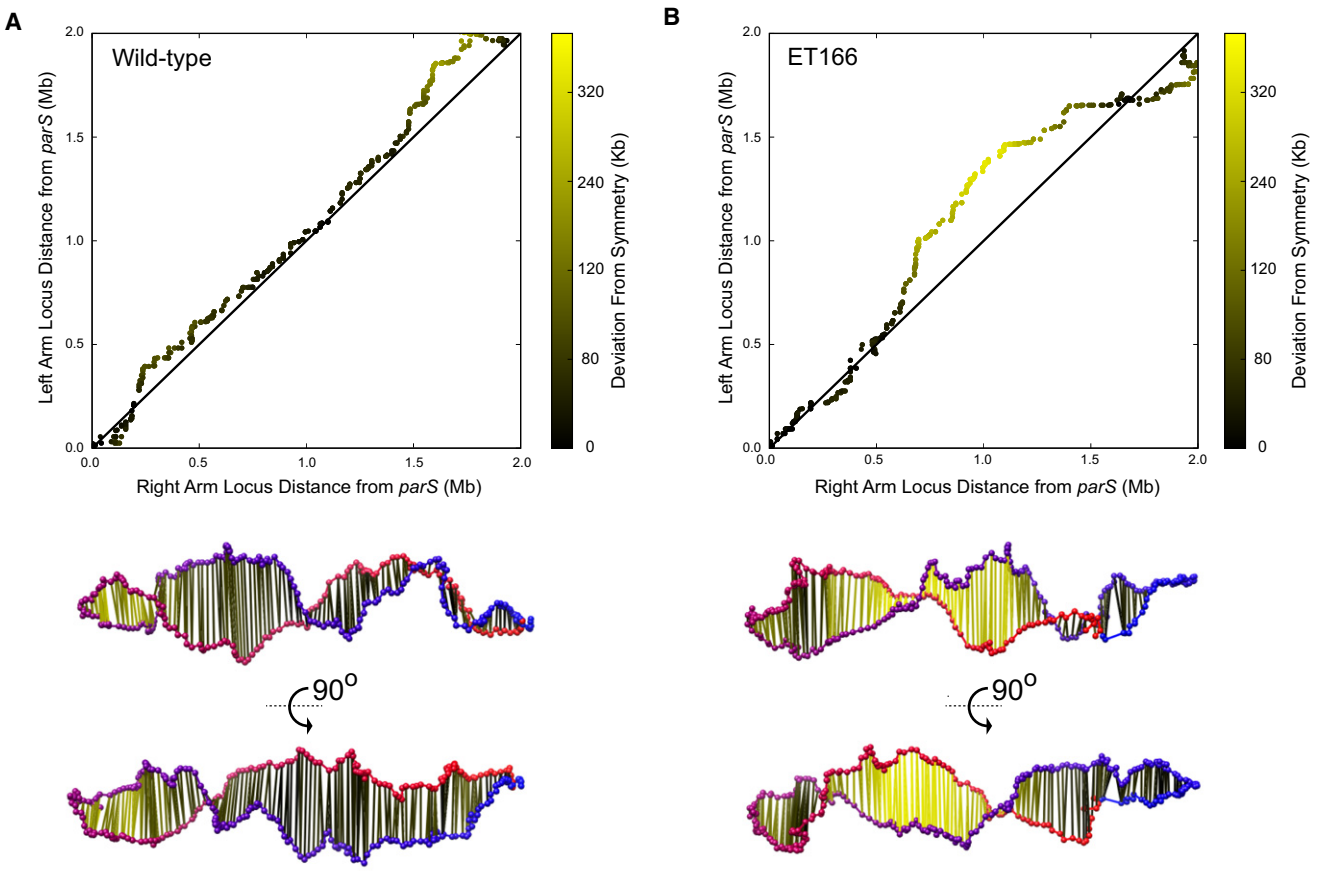

Figure 5. Interarm Alignments Reveal Interaction Asymmetries in ET166 Swarmer Cells

(A) Top: Wild-type cluster 1 swarmer long-axis alignment plot. The genomic distance of each fragment to the most polar fragment (*parS* elements) is plotted against the genomic distance of the closest opposite arm fragment (with respect to position along the long axis of the models) to this same maximally polar fragment. The black line indicates a perfectly symmetric pairing, and increasingly yellow colors indicate larger deviations from symmetry. Data represent the median for 200 random cluster 1 models. Bottom: 3D representation of the long-axis alignment in wild-type swarmer cells using the smoothed centroid of cluster 1. Nearest neighbor opposite-arm fragments are connected by lines whose colors indicate the degree of deviation from symmetry.

(B) Top: ET166 cluster 1 long-axis alignment plot. Bottom: 3D representation of the ET166 alignment utilizing the smoothed centroid model from cluster 1. A similar plot for ET163 can be found in Figure S5.

asymmetry would not be expected if polar localization alone rendered a region compact. Thus, we conclude that the *parS* sites nucleate a compact chromosome conformation that spreads 100–200 kb into flanking genomic regions.

The Swarmer Cell Chromosome Is Free to Rotate about the Long Axis of the Cell

The results described above reveal that there are strong constraints on locus positioning along the long axis of the cell. We next set out to explore whether similar constraints are present along the short axis by assessing if the *Caulobacter* chromosome is free to rotate about the long axis of the cell. We constructed three double-label strains in which the markers were located on opposite arms at similar genomic distances from the *parS* elements (Figures 7A). We then determined the number of cells in which each arm was closest to the ventral side of the cell and found that the queried loci did not preferentially localize to a given side of the swarmer cell (Figures 7A and S6). To confirm this finding, we also analyzed a large set of strains in which a single locus was labeled. We expected that if the arms of the chromosome do in fact reside on a particular side of the cell, the distributions of the positioning of such loci along the short axis of the cell would reveal such a preferential localization pattern. However, the distributions of 38 markers at unique chromosomal sites in a total of ~200,000 cells illustrate that the arms were equivalently distributed about the short axis of the cell (Figure 7B). Thus, our results demonstrate that while the *Caulobacter* chromosome is oriented along the long axis of the cell through the action of the *parS* elements, there is no such organization along the short axis, and instead the chromosome is free to rotate about the long axis of the cell.

DISCUSSION

Our contact-based 3D models and fluorescent microscopy illustrate that the *parS* sites define the global structure of the

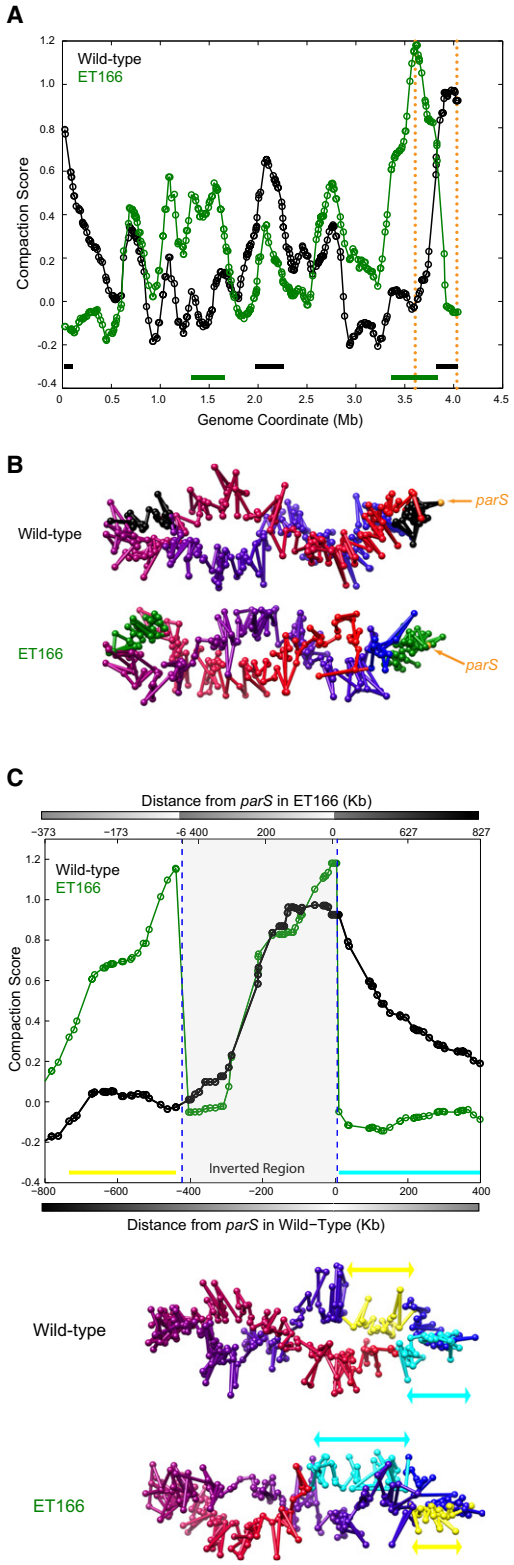

Figure 6. The *parS* Sites and Polar Localization Contribute to the Formation of Compact Chromatin

(A) Top: Wild-type (black) and ET166 (green) genome compaction profiles for cluster 1 models. Local compaction (derived from the 3D distances between neighboring restriction fragments) is plotted against genome position (Supplemental Experimental Procedures). The genome coordinates of restriction fragments in ET166 have been adjusted to account for the inversion present in this strain. Dashed orange lines indicate the positions of the *parS* sites. Green and black bars indicate the regions highlighted below.

(B) The centroid models of wild-type and ET166 cluster 1, with color indicating the pole-proximal regions determined to be particularly compact (see A).

(C) Top: Plot of compaction versus genomic distance from the *parS* sites for wild-type (black) and ET166 (green) model clusters. Fragments are ordered along the horizontal axis according to their positions in the wild-type genome. Dashed blue lines denote the inversion break points. In ET166, the shaded region is inverted such that the rightmost edge of the shaded region lies adjacent to the region to the left of the left dashed blue line. Absolute distances of fragments from the *parS* elements in the wild-type and ET166 genome are indicated by the horizontal axes at bottom and top, respectively, with the horizontal color bars indicating absolute distance from the *parS* sites. Yellow and cyan lines denote genomic regions that are more compact in ET166 and wild-type, respectively. These regions are highlighted on the centroid models from the wild-type and ET166 model cluster 1 (bottom).

Caulobacter genome. Our data indicate that these sites reside at the pole of the wild-type swarmer chromosome/cell and that moving a 10 kb region containing them elsewhere in the genome yields large-scale rotations of the chromosome that reposition these elements at the cell/structural pole. The *parS* sites are conserved sequence elements present within 69% of sequenced bacterial genomes (Livny et al., 2007) and segregate first regardless of their genomic positions (Toro et al., 2008). In addition, evidence suggests they anchor the chromosome to the pole via interactions with the ParB and PopZ proteins (Bowman et al., 2008; Ebersbach et al., 2008). We therefore propose that our findings are a consequence of the *parS* sites being the first genomic elements to segregate to the opposite pole, where they become anchored and thereby establish the global orientation of the genome. Such a model is supported by the fact that in both wild-type and ET166 cells, loci segregate in an order roughly corresponding to their genomic distances from the *parS* sites (Viollier et al., 2004). Thus, our findings indicate that the global orientation of the chromosome may be defined by the order of segregation and that the rotated global arrangements of the genome observed in inversion strains ET166 and ET322 are the result of a perturbation of the order of segregation of loci that results from the repositioning of the *parS* sites.

In addition to shaping the global orientation of the *Caulobacter* genome, we show that the *parS* sites also nucleate a compact chromatin conformation over ~100 kb, as moving these elements elsewhere in the genome condenses the regions placed near these sites and decondenses the regions moved away. Although our data indicate that polar localization alone induces the formation of compact chromatin, the *parS* sites yield a particularly compact conformation. We hypothesize that that is due to interactions with ParB, which itself is thought to physically interact with structural maintenance of chromosomes (SMC), a protein known to play a role in chromosome compaction and segregation across a number bacterial species, including *Caulobacter* (Britton et al., 1998; Jensen and Shapiro, 1999; Wang et al., 2006a). Consistent with such an explanation, it has been demonstrated that in *Bacillus subtilis*, ParB (SpoOj) spreads from the *parS* sites into adjacent regions of the genome (Breier and Grossman, 2007) and recruits the SMC complex to

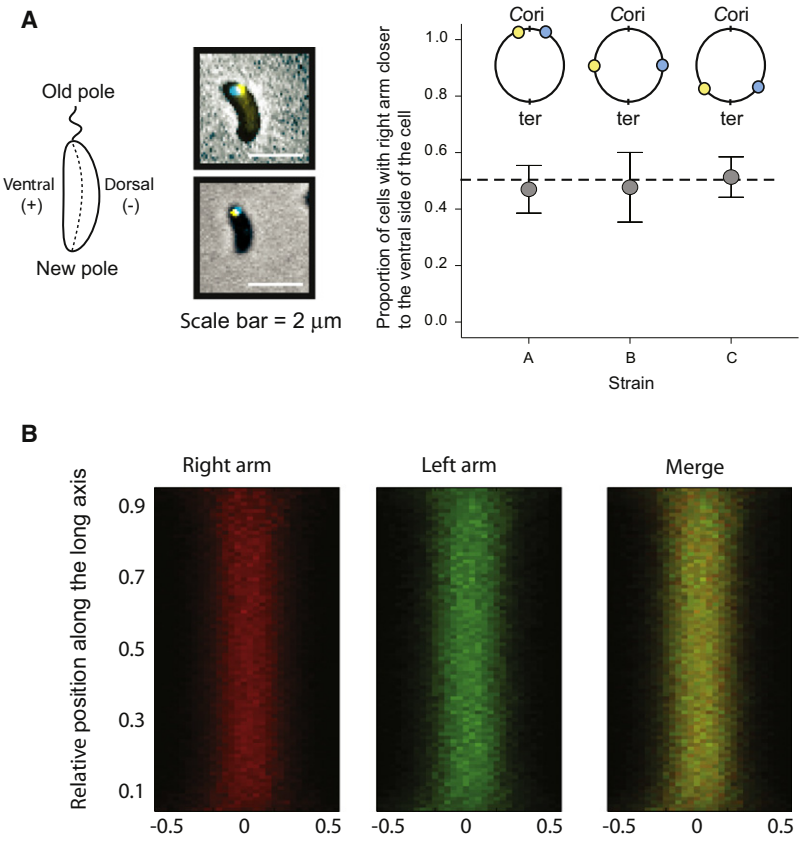

Figure 7. The *Caulobacter* Chromosome Is Free to Rotate around the Long Cell Axis

(A) Left: Schematic of a *Caulobacter* swarmer cell indicating the positions of the new and old poles as well as the dorsal and ventral sides of the cell. Negative and positive signs refer to the convention used by our image analysis software. Center: Example micrographs of double-labeled *Caulobacter* swarmer cells showing configurations of the chromosome in which the labeled loci reside on opposite sides of the cell. Right: Relative positions of the left- and right-arm markers in three strains marked at different positions in the chromosome. Circles denote the means of three experiments, each of which included at least 400 cells. Bars represent 95% confidence intervals of the mean. The dotted line indicates the expected value for a distribution in which loci have no preferential localization along the short axis.

(B) Virtual cell showing the distribution of ~200,000 LacI-CFP foci along the short and long axes of the cell. Left: Markers on the right arm. Center: Markers on the left arm. Right: Merge of the two arms. Note that the two arms are equally distributed along the short cell axis.

these regions (Gruber and Errington, 2009; Sullivan et al., 2009). Thus, the data presented here, which demonstrate that the centromeric region of a bacterial chromosome is particularly compact in vivo, connect SMC's previously noted effects upon chromosome segregation and compaction.

Our models also elucidate the detailed arrangement of the arms of the chromosome and demonstrate that the chromosomal arms are arranged in a periodic fashion. Interestingly, a helical arrangement of newly replicated DNA has been observed in *B. subtilis* (Berlatzky et al., 2008). While the mechanism behind such a periodic arrangement in *Caulobacter* and/or *B. subtilis* is yet to be unraveled, such arrangements could represent an energetic minimum (Maritan et al., 2000). Alternatively, these highly regular folding patterns could be the consequence of interactions between the genome and helically arranged cytoskeletal proteins such as MreB (Gitai and Shapiro, 2003).

We find that opposite-arm loci equidistant from the *parS* elements are aligned at similar positions along the long axis of the wild-type swarmer cell chromosome structure. However, the inversions in strains ET163 and ET166 yield regions of the structure in which opposite-arm loci are no longer well aligned. These misalignments suggest that there are additional constraints on the positioning of loci along the long axis of the structure/cell. In keeping with the segregation-based model posed above, the inversions in strains ET163 and ET166 could affect the timing of segregation of opposite arm loci and thereby influence the alignment and positioning of the arms of the chromosome.

Our microscopy studies indicate that loci have no preferential locations about the short axis of the cell and therefore that the chromosome has no preferential orientation about this axis. Therefore, the *parS* sites represent the only sequence elements that stably anchor the chromosome to the cell. Such a finding is consistent with recent simulations, which have illustrated that anchoring near the origin alone is sufficient to yield the overall linear arrangement of loci observed in swarmer cells (Buenemann and Lenz, 2010). However, it remains possible that events such as transertion (Woldringh, 2002), the simultaneous transcription, translation, and insertion of membrane proteins into the cellular envelope, may transiently couple the genome to the membrane.

In eukaryotes the subnuclear localization of genes is sometimes correlated with their expression (Andrulis et al., 1998; Kosak et al., 2002). In most cases cause-and-effect relationships for these correlations are unclear. In cases where the subnuclear position of a gene could be experimentally altered, the resulting gene expression changes were small (Finlan et al., 2008; Kumaran and Spector, 2008). Our observation that genome-wide rotation resulting from relocalization of the *parS* sites did not dramatically alter gene expression is in line with these eukaryotic studies. Although a number of genes were affected, the effect was typically less than 2-fold. Thus, the precise position of a gene along the long axis of the cell does not strongly influence its expression. Additionally, it is unlikely that the perturbed genome conformations observed in our inversion strains are the result of large-scale transcriptional changes. Instead, the structural changes observed in the strains are likely the result of changes in the order of loci segregation caused by the movement of the *parS* sites.

The work presented here illustrates how a comprehensive study of genome 3D architecture can provide insight into the roles of sequence elements and fundamental DNA-based processes

in defining this structure. The experimental paradigm we introduce is general and could be used in conjunction with genetic perturbations to elucidate the roles of nucleoid-associated proteins, *cis*-elements, and DNA-templated processes such as transcription and replication in shaping the folding of the genome. With additional advances, including decreases in DNA sequencing costs, such a paradigm could also be applied to larger eukaryotic genomes to further elucidate the complex relationships between genome sequence, structure, and function.

EXPERIMENTAL PROCEDURES

More detailed experimental procedures, including descriptions of our inversion strain construction, polony sequencing, model generation, 5C data/model analysis, live-cell imaging, and microarray procedures can be found in the Supplemental Experimental Procedures.

Chromosome Conformation Capture

Synchronous swarmer cells were isolated as previously described (Alley et al., 1993) and were crosslinked with 1.0% formaldehyde. Cells were pelleted, resuspended in 1× TE at a concentration of 1 × 10^7 cells/microliter, and lysed with Ready-Lyse (Epicenter) lysozyme (20 U/μl). Cells were then solubilized with 0.5% SDS, and chromatin was digested with BglII (0.94 U/μl) in 1× buffer 3 (New England Biolabs) containing 1.0% Triton X-100. Digested chromatin was solubilized using SDS (0.9%) and was ligated at a final concentration of 0.25 ng/μl in 1× T4 DNA ligase buffer containing 1% Triton X-100. 3C libraries were purified via phenol-chloroform extraction and ethanol precipitation.

Chromosome Conformation Capture Carbon Copy

Melting temperature-normalized probes were designed such that their sequence was complementary to the sequence upstream of BglII restriction sites, with adjacent probes containing sequence corresponding to opposite strands (plus versus minus). Plus-strand probes were flanked by the forward emulsion PCR primer (see Supplemental Experimental Procedures), and minus-strand probes were flanked by the reverse complement of the reverse emulsion PCR primer. 3C libraries (1.8 ng/μl) were denatured at 95°C for 10 min in 1× AMP ligase buffer, probes were annealed for 14 hr at 65°C at a concentration of 0.2 nM (per probe), and ligation was subsequently performed at 65°C for 1 hr using AMP ligase (0.0167 U/μl). Ligated probes were amplified via PCR.

ACCESSION NUMBERS

Both raw and processed microarray data were deposited in the Gene Expression Omnibus (accession number GSE31468).

SUPPLEMENTAL INFORMATION

Supplemental Information includes six figures, nine tables, Supplemental Experimental Procedures, and Supplemental References and can be found with this article online at doi:10.1016/j.molcel.2011.09.010.

ACKNOWLEDGMENTS

We acknowledge Tony Tsai for preliminary microscopy data and Marian Walhout, Zhiping Weng, Andrew Tolonen, John Aach, Jae Kim, Kun Zhang, Sara Vassallo, and Nikos Reppas for helpful suggestions/reading of the manuscript. We thank Barrett Perchuk and Michael Laub for help with the microarray experiments. We thank the IMP community (http://www.integrativemodeling.org/), especially Daniel Russell, Ben Webb, and Andrej Sali, and the Chimera developers (http://www.cgl.ucsf.edu/chimera/), including Thomas Goddard and Tom Ferrin. Work conducted by M.A.U., M.A.W., G.J.P., and G.M.C. was supported by a Department of Energy GTL center grant (to G.M.C.). E.T. was partially supported by the Smith Stanford Graduate Fellowship, and L.S. was supported by National Institutes of Health grants R01 GM51426 and R24 GM073011-04. M.A.M.-R. was funded by the Spanish Ministerio de Ciencia e Innovación (BIO2007/66670 and BFU2010/19310), and J.D. was supported by a grant from the National Institutes of Health (HG003143) and a W.M. Keck Foundation Distinguished Young Scholar Award.

Received: October 26, 2010
Revised: August 1, 2011
Accepted: September 15, 2011
Published: October 20, 2011

REFERENCES

Alber, F., Dokudovskaya, S., Veenhoff, L.M., Zhang, W., Kipper, J., Devos, D., Suprapto, A., Karni-Schmidt, O., Williams, R., Chait, B.T., et al. (2007). Determining the architectures of macromolecular assemblies. Nature *450*, 683–694.

Alley, M.R., Maddock, J.R., and Shapiro, L. (1993). Requirement of the carboxyl terminus of a bacterial chemoreceptor for its targeted proteolysis. Science *259*, 1754–1757.

Andrulis, E.D., Neiman, A.M., Zappulla, D.C., and Sternglanz, R. (1998). Perinuclear localization of chromatin facilitates transcriptional silencing. Nature *394*, 592–595.

Baù, D., Sanyal, A., Lajoie, B.R., Capriotti, E., Byron, M., Lawrence, J.B., Dekker, J., and Marti-Renom, M.A. (2011). The three-dimensional folding of the α-globin gene domain reveals formation of chromatin globules. Nat. Struct. Mol. Biol. *18*, 107–114.

Berlatzky, I.A., Rouvinski, A., and Ben-Yehuda, S. (2008). Spatial organization of a replicating bacterial chromosome. Proc. Natl. Acad. Sci. USA *105*, 14136–14140.

Bowman, G.R., Comolli, L.R., Zhu, J., Eckart, M., Koenig, M., Downing, K.H., Moerner, W.E., Earnest, T., and Shapiro, L. (2008). A polymeric protein anchors the chromosomal origin/ParB complex at a bacterial cell pole. Cell *134*, 945–955.

Breier, A.M., and Grossman, A.D. (2007). Whole-genome analysis of the chromosome partitioning and sporulation protein Spo0J (ParB) reveals spreading and origin-distal sites on the Bacillus subtilis chromosome. Mol. Microbiol. *64*, 703–718.

Britton, R.A., Lin, D.C., and Grossman, A.D. (1998). Characterization of a prokaryotic SMC protein involved in chromosome partitioning. Genes Dev. *12*, 1254–1259.

Buenemann, M., and Lenz, P. (2010). A geometrical model for DNA organization in bacteria. PLoS ONE *5*, e13806.

Dekker, J. (2008). Gene regulation in the third dimension. Science *319*, 1793–1794.

Dekker, J., Rippe, K., Dekker, M., and Kleckner, N. (2002). Capturing chromosome conformation. Science *295*, 1306–1311.

Dostie, J., Richmond, T.A., Arnaout, R.A., Selzer, R.R., Lee, W.L., Honan, T.A., Rubio, E.D., Krumm, A., Lamb, J., Nusbaum, C., et al. (2006). Chromosome Conformation Capture Carbon Copy (5C): a massively parallel solution for mapping interactions between genomic elements. Genome Res. *16*, 1299–1309.

Duan, Z., Andronescu, M., Schutz, K., McIlwain, S., Kim, Y.J., Lee, C., Shendure, J., Fields, S., Blau, C.A., and Noble, W.S. (2010). A three-dimensional model of the yeast genome. Nature *465*, 363–367.

Ebersbach, G., Briegel, A., Jensen, G.J., and Jacobs-Wagner, C. (2008). A self-associating protein critical for chromosome attachment, division, and polar organization in caulobacter. Cell *134*, 956–968.

Elmore, S., Müller, M., Vischer, N., Odijk, T., and Woldringh, C.L. (2005). Single-particle tracking of oriC-GFP fluorescent spots during chromosome segregation in Escherichia coli. J. Struct. Biol. *151*, 275–287.

Fiebig, A., Keren, K., and Theriot, J.A. (2006). Fine-scale time-lapse analysis of the biphasic, dynamic behaviour of the two Vibrio cholerae chromosomes. Mol. Microbiol. *60*, 1164–1178.

Finlan, L.E., Sproul, D., Thomson, I., Boyle, S., Kerr, E., Perry, P., Ylstra, B., Chubb, J.R., and Bickmore, W.A. (2008). Recruitment to the nuclear periphery can alter expression of genes in human cells. PLoS Genet. *4*, e1000039.

Fullwood, M.J., Liu, M.H., Pan, Y.F., Liu, J., Xu, H., Mohamed, Y.B., Orlov, Y.L., Velkov, S., Ho, A., Mei, P.H., et al. (2009). An oestrogen-receptor-alpha-bound human chromatin interactome. Nature *462*, 58–64.

Gheldof, N., Tabuchi, T.M., and Dekker, J. (2006). The active FMR1 promoter is associated with a large domain of altered chromatin conformation with embedded local histone modifications. Proc. Natl. Acad. Sci. USA *103*, 12463–12468.

Gilbert, N., Boyle, S., Fiegler, H., Woodfine, K., Carter, N.P., and Bickmore, W.A. (2004). Chromatin architecture of the human genome: gene-rich domains are enriched in open chromatin fibers. Cell *118*, 555–566.

Gitai, Z., and Shapiro, L. (2003). Bacterial cell division spirals into control. Proc. Natl. Acad. Sci. USA *100*, 7423–7424.

Gruber, S., and Errington, J. (2009). Recruitment of condensin to replication origin regions by ParB/SpoOJ promotes chromosome segregation in B. subtilis. Cell *137*, 685–696.

Jensen, R.B. (2006). Analysis of the terminus region of the Caulobacter crescentus chromosome and identification of the dif site. J. Bacteriol. *188*, 6016–6019.

Jensen, R.B., and Shapiro, L. (1999). The Caulobacter crescentus smc gene is required for cell cycle progression and chromosome segregation. Proc. Natl. Acad. Sci. USA *96*, 10661–10666.

Jun, S., and Mulder, B. (2006). Entropy-driven spatial organization of highly confined polymers: lessons for the bacterial chromosome. Proc. Natl. Acad. Sci. USA *103*, 12388–12393.

Kosak, S.T., Skok, J.A., Medina, K.L., Riblet, R., Le Beau, M.M., Fisher, A.G., and Singh, H. (2002). Subnuclear compartmentalization of immunoglobulin loci during lymphocyte development. Science *296*, 158–162.

Kumaran, R.I., and Spector, D.L. (2008). A genetic locus targeted to the nuclear periphery in living cells maintains its transcriptional competence. J. Cell Biol. *180*, 51–65.

Lieberman-Aiden, E., van Berkum, N.L., Williams, L., Imakaev, M., Ragoczy, T., Telling, A., Amit, I., Lajoie, B.R., Sabo, P.J., Dorschner, M.O., et al. (2009). Comprehensive mapping of long-range interactions reveals folding principles of the human genome. Science *326*, 289–293.

Livny, J., Yamaichi, Y., and Waldor, M.K. (2007). Distribution of centromere-like parS sites in bacteria: insights from comparative genomics. J. Bacteriol. *189*, 8693–8703.

Maritan, A., Micheletti, C., Trovato, A., and Banavar, J.R. (2000). Optimal shapes of compact strings. Nature *406*, 287–290.

Mercier, R., Petit, M.A., Schbath, S., Robin, S., El Karoui, M., Boccard, F., and Espéli, O. (2008). The MatP/matS site-specific system organizes the terminus region of the E. coli chromosome into a macrodomain. Cell *135*, 475–485.

Miele, A., Bystricky, K., and Dekker, J. (2009). Yeast silent mating type loci form heterochromatic clusters through silencer protein-dependent long-range interactions. PLoS Genet. *5*, e1000478.

Mohl, D.A., and Gober, J.W. (1997). Cell cycle-dependent polar localization of chromosome partitioning proteins in Caulobacter crescentus. Cell *88*, 675–684.

Nielsen, H.J., Ottesen, J.R., Youngren, B., Austin, S.J., and Hansen, F.G. (2006). The Escherichia coli chromosome is organized with the left and right chromosome arms in separate cell halves. Mol. Microbiol. *62*, 331–338.

Postow, L., Hardy, C.D., Arsuaga, J., and Cozzarelli, N.R. (2004). Topological domain structure of the Escherichia coli chromosome. Genes Dev. *18*, 1766–1779.

Reyes-Lamothe, R., Possoz, C., Danilova, O., and Sherratt, D.J. (2008). Independent positioning and action of Escherichia coli replisomes in live cells. Cell *133*, 90–102.

Shendure, J., Porreca, G.J., Reppas, N.B., Lin, X., McCutcheon, J.P., Rosenbaum, A.M., Wang, M.D., Zhang, K., Mitra, R.D., and Church, G.M. (2005). Accurate multiplex polony sequencing of an evolved bacterial genome. Science *309*, 1728–1732.

Simonis, M., Klous, P., Splinter, E., Moshkin, Y., Willemsen, R., de Wit, E., van Steensel, B., and de Laat, W. (2006). Nuclear organization of active and inactive chromatin domains uncovered by chromosome conformation capture-on-chip (4C). Nat. Genet. *38*, 1348–1354.

Sullivan, N.L., Marquis, K.A., and Rudner, D.Z. (2009). Recruitment of SMC by ParB-parS organizes the origin region and promotes efficient chromosome segregation. Cell *137*, 697–707.

Teleman, A.A., Graumann, P.L., Lin, D.C., Grossman, A.D., and Losick, R. (1998). Chromosome arrangement within a bacterium. Curr. Biol. *8*, 1102–1109.

Thanbichler, M., and Shapiro, L. (2006a). Chromosome organization and segregation in bacteria. J. Struct. Biol. *156*, 292–303.

Thanbichler, M., and Shapiro, L. (2006b). MipZ, a spatial regulator coordinating chromosome segregation with cell division in Caulobacter. Cell *126*, 147–162.

Tolhuis, B., Palstra, R.J., Splinter, E., Grosveld, F., and de Laat, W. (2002). Looping and interaction between hypersensitive sites in the active beta-globin locus. Mol. Cell *10*, 1453–1465.

Toro, E., Hong, S.H., McAdams, H.H., and Shapiro, L. (2008). Caulobacter requires a dedicated mechanism to initiate chromosome segregation. Proc. Natl. Acad. Sci. USA *105*, 15435–15440.

Vernimmen, D., De Gobbi, M., Sloane-Stanley, J.A., Wood, W.G., and Higgs, D.R. (2007). Long-range chromosomal interactions regulate the timing of the transition between poised and active gene expression. EMBO J. *26*, 2041–2051.

Viollier, P.H., Thanbichler, M., McGrath, P.T., West, L., Meewan, M., McAdams, H.H., and Shapiro, L. (2004). Rapid and sequential movement of individual chromosomal loci to specific subcellular locations during bacterial DNA replication. Proc. Natl. Acad. Sci. USA *101*, 9257–9262.

Wang, Q., Mordukhova, E.A., Edwards, A.L., and Rybenkov, V.V. (2006a). Chromosome condensation in the absence of the non-SMC subunits of MukBEF. J. Bacteriol. *188*, 4431–4441.

Wang, X., Liu, X., Possoz, C., and Sherratt, D.J. (2006b). The two Escherichia coli chromosome arms locate to separate cell halves. Genes Dev. *20*, 1727–1731.

White, M.A., Eykelenboom, J.K., Lopez-Vernaza, M.A., Wilson, E., and Leach, D.R. (2008). Non-random segregation of sister chromosomes in Escherichia coli. Nature *455*, 1248–1250.

Woldringh, C.L. (2002). The role of co-transcriptional translation and protein translocation (transertion) in bacterial chromosome segregation. Mol. Microbiol. *45*, 17–29.

Zhao, Z., Tavoosidana, G., Sjölinder, M., Göndör, A., Mariano, P., Wang, S., Kanduri, C., Lezcano, M., Sandhu, K.S., Singh, U., et al. (2006). Circular chromosome conformation capture (4C) uncovers extensive networks of epigenetically regulated intra- and interchromosomal interactions. Nat. Genet. *38*, 1341–1347.